# Remarkably Strong Interparticle Coupling in Two-Dimensional Ensembles of Naked Silver Quantum Dots: The Effect on Optical and Conduction Characteristics

**ARTICLE** *in* THE JOURNAL OF PHYSICAL CHEMISTRY C · MARCH 2009

Impact Factor: 4.77 · DOI: 10.1021/jp808516f



**2 AUTHORS**, INCLUDING:

Shiliang Wang
Suffield Research Centre
**39** PUBLICATIONS **345** CITATIONS

THE JOURNAL OF PHYSICAL CHEMISTRY C



Article

# Remarkably Strong Interparticle Coupling in Two-Dimensional Ensembles of *Naked* Silver Quantum Dots: The Effect on Optical and Conduction Characteristics

David B. Pedersen, and Shiliang Wang

*J. Phys. Chem. C*, **2009**, 113 (12), 4797-4803• DOI: 10.1021/jp808516f • Publication Date (Web): 03 March 2009



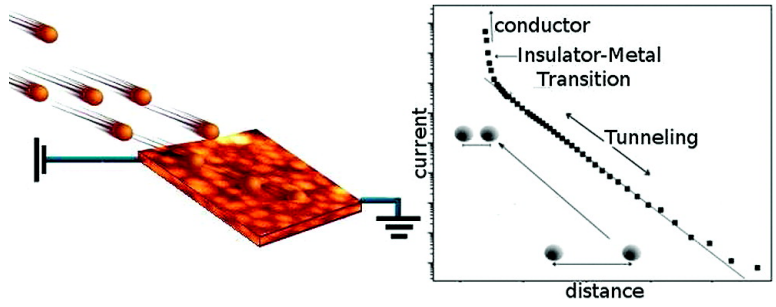


## More About This Article

Additional resources and features associated with this article are available within the HTML version:

- Supporting Information
- Access to high resolution figures
- Links to articles and content related to this article
- Copyright permission to reproduce figures and/or text from this article

View the Full Text HTML

# Remarkably Strong Interparticle Coupling in Two-Dimensional Ensembles of *Naked* Silver Quantum Dots: The Effect on Optical and Conduction Characteristics

**David B. Pedersen* and Shiliang Wang**

*Defence R&D Canada-Suffield, Suffield, Alberta, T1A 8K6, Canada*

*Received: September 25, 2008; Revised Manuscript Received: January 13, 2009*

Tunable two-dimensional ensembles of naked silver quantum dots have been assembled, using gas-phase deposition techniques, and their conduction and optical characteristics have been measured. With decreasing interparticle separation, the optical properties are found to evolve from particle-like to bulk metal-like. Two conduction mechanisms are found. At relatively large interparticle separations, interparticle tunneling of charge is prominent. At relatively small separations, we propose that resonant charge transport through the quantum dot ensembles occurs. Because the quantum dots are naked, these results provide new insight into particle−particle coupling interactions, specifically, which are much stronger than those observed in the ligated nanoparticle film systems that are typically studied. Tunneling current is observed over remarkably large average interparticle separations (greater than 40 nm), and surface plasmon resonances are shifted more than 1.7 eV as a result of the strong interparticle coupling. Because of stronger coupling, we also find that the ensemble-dependent band gap can be tuned from 0 to ∼5 V over a larger range of interparticle separations than possible in the ligated nanoparticle film systems.

## 1. Introduction

Tunability of conduction characteristics is a key aspect of next generation, nanoparticle-based electronic devices. In this context, ensembles of quantum dots are promising because they can be tuned from resistor to conductor simply by varying the interparticle spacing. This distance dependence of the conductance constitutes the foundation on which our understanding of Mott insulator-to-metal transitions (MIMTs) is built.[1,2] In recent years, studies of the evolution of the conduction characteristics of quantum dot ensembles have revealed a rich conductance consisting of multiple spacing-dependent conduction mechanisms (e.g., work by Heath's group).[3−5] These include tunneling, variable range hopping, insulator to metal transition, and Anderson localization.[6] In addition to the variety of mechanisms, Coulomb blockade effects associated with the finite charging energies of nanoparticles also impact the conductance characteristics. Adding to the complexity is the fact that different stabilizer ligands, used for quantum dot synthesis to control dot size and to prevent quantum dot coalescence, can manifest different conduction and optical characteristics by damping the interparticle coupling. The realization of ideal systems where conductance can be interpreted strictly in terms of distance-dependent interactions between *naked* particles in an extended quantum dot ensemble is therefore desirable, as it establishes a ligand-free benchmark system.

Here, we describe the realization of two-dimensional ensembles of ligand-free quantum dots and in situ measurements of their conductance during formation of the ensembles via deposition of Ag quantum dots onto glass substrates under vacuum conditions. The deposition process yields ensembles with average interparticle spacings that decrease steadily as a function of deposition time. Accordingly, the conductance characteristics of ligand-free quantum dot ensembles have been measured over a comprehensive range of distances from relatively large, where the onset of tunneling current is observed, to the close-packed quantum dot solid, which is conducting. Because the quantum dots are naked, coupling interactions between adjacent dots are not damped by ligands and occur at relatively long distances. Optical data suggest that coupling is strong enough to give metallic character to the ensembles. The fact that such near-metallic behavior has not been observed in ligated nanoparticle film systems without severe compression of the film to interparticle separations of less than 1.5 nm attests to the magnitude of the interparticle coupling effects that are prevalent in the naked nanoparticle films.

## 2. Experimental Section

To prepare assemblies of Ag quantum dots, we employed a system that generates gas-phase Ag quantum dots in a vacuum environment and deposits these onto substrates.[7] The substrates used include glass and highly ordered pyrolytic graphite (HOPG) to which the quantum dots were found to stick readily. The apparatus for preparation of assemblies of quantum dots is illustrated in Figure 1.[7] In this procedure, application of a 270−300 V bias between the anode cap and a metal target causes a discharge in the 0.17 Torr pressure of Ar gas maintained between them. The $Ar^+$ ions generated are accelerated toward the negatively biased metal target, which they strike with force, thus liberating metal atoms to the gas phase. These atoms are swept up in the flow of Ar leaving the discharge region. The Ar flows because of the pressure differential maintained by vacuum pumps positioned downstream from the metal sputtering region. Upon leaving the sputtering region, the atoms pass through an aggregation zone where the collision frequency is high, collisions between metal atoms frequent, and formation of quantum dots occurs. The quantum dots then expand through a 5 mm orifice into the deposition chamber where the pressure is low enough that particle growth is terminated. A substrate positioned in front of the orifice collects the quantum dots, which deposit as a two-dimensional film. From scanning tunneling

* To whom correspondence should be addressed. E-mail: david.pedersen@drdc-rddc.gc.ca.

10.1021/jp808516f CCC: $40.75 Published 2009 by the American Chemical Society
Published on Web 03/03/2009

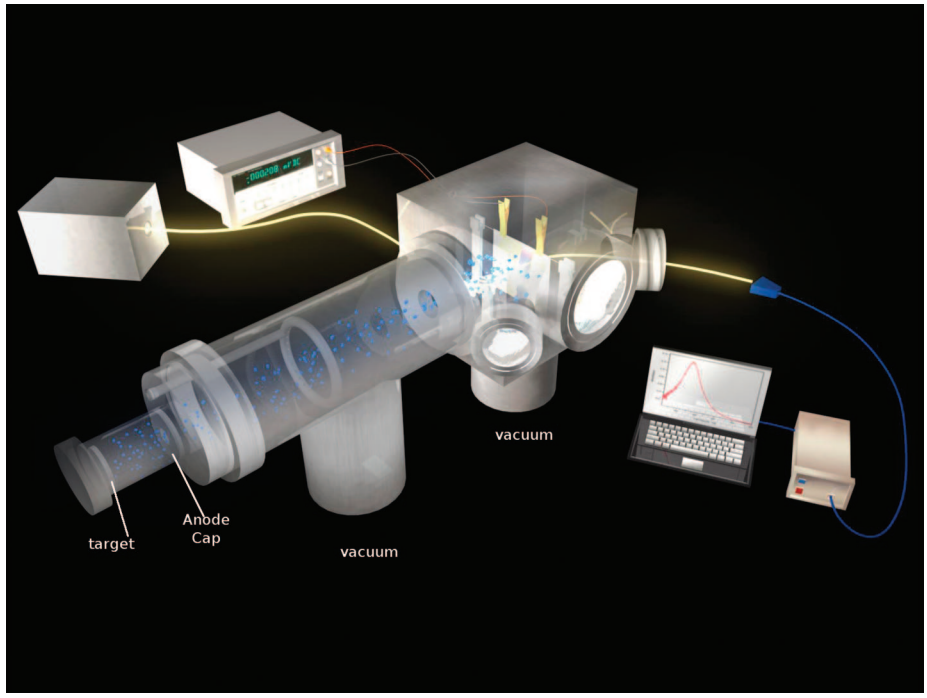


**Figure 1.** Schematic of the quantum dot film preparation apparatus. See text for details.

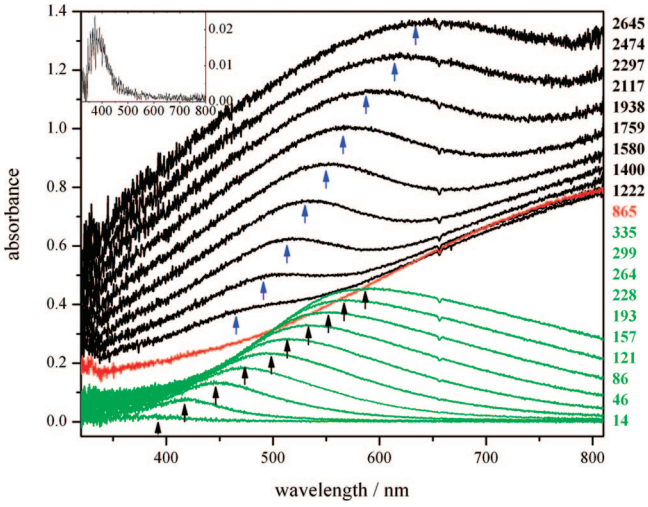


**Figure 2.** Absorbance spectra collected at various times during deposition of a Ag quantum dot film onto a glass substrate. The times at which the spectra were collected are shown along the right axis. Times are given in seconds with the start of deposition being 0 s. The inset is a magnification of the earliest spectrum (14 s) where the position of the plasmon band at 380 ± 5 nm can be seen clearly. Green spectra correspond to the first monolayer, red correpond to the film reaching constant resistance (completed monolayer), and black spectra show the reappearance of the surface plasmon resonance, which is attributed to the second monolayer deposited atop the first. The position of the surface plasmon of the first monolayer is labeled with black arrows, with blue arrows for the second monolayer.

microscope images of the quantum dots deposited on HOPG, like that shown in the inset of Figure 4, the size of the quantum dots was found to be 3.0 ± 0.5 nm in diameter. The quantum dots were monodispersed, as seen in Figure 4. An interesting feature of this approach is that the spacing between the particles varies systematically with deposition time; at longer times, more particles reside on the surface and the average interparticle spacing is decreased accordingly.[8] Previous work has demonstrated a linear correlation between the average interparticle spacing and $t^{-1/2}$, where $t$ is the deposition time.[9] To measure conductance characteristics, electrodes 3 mm apart were painted onto glass substrates using silver paint (SPI) and allowed to cure. The quantum dot film was then deposited on top of the electrodes. The current flow between electrodes was monitored with an electrochemical work station (CH Instruments, CHI660C) as deposition proceeded. Periodically, the deposition was stopped and current−voltage ($I-V$) scans were acquired. In situ optical measurements were made concurrently by passing the light from a halogen/deuterium lamp (coupled into the vacuum system via an optic fiber feedthrough) through the quantum dot film and glass substrate and passing the transmitted light into a spectrometer (Ocean Optics SD2000) during deposition.

## 3. Results and Discussion

Monitoring the optical properties of the quantum dots in situ during deposition provides significant insight into the nature of the films produced and the type of growth mechanism at work. Sample absorption spectra collected at various times during deposition of a Ag quantum dot film are shown in Figure 2. At the earliest deposition times, the spectrum has a prominent peak at 380 ± 5 nm. This is the surface plasmon resonance (SPR) absorption expected of isolated Ag quantum dots with diameters of less than 10 nm.[10,11] As the deposition proceeds, this peak increases in height, due to the increasing number of quantum dots, and after a short time (~30 s), it starts shifting steadily to longer wavelengths (green spectra). From Figure 3, the interparticle spacing is 50 ± 15 nm when the shifting begins. The shift is caused by dipolar coupling between quantum dots.[12−14] The coupling effect is distance-dependent and the continuous shifting reflects the continuous decrease in average interparticle spacing that occurs as the number of particles on the surface steadily increases. At 865 s (red spectrum), the SPR absorption is no longer prominent, and the spectrum is rather featureless and resembles the spectrum of a solid film of Ag metal.[15,16] Note, however, that this material is not bulk silver metal but rather a conducting assembly of isolated naked Ag quantum dots. This fact becomes evident as more particles are added to the assembly at which time, as seen in Figure 2, the surface

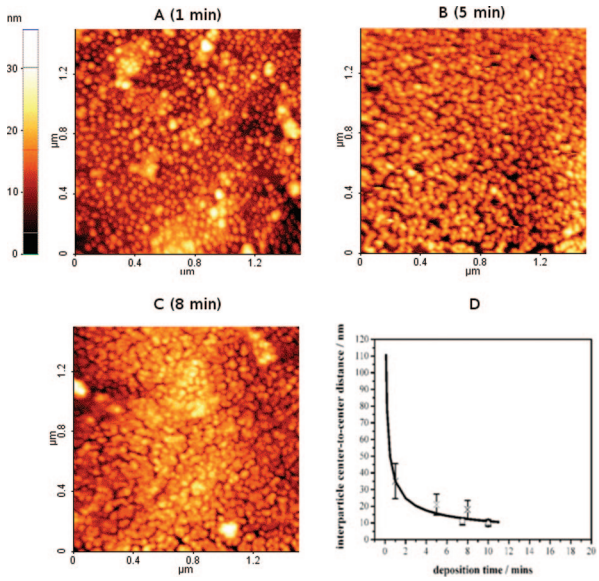


**Figure 3.** AFM images showing the topography of Ag nanoparticles deposited on HOPG are shown for 1, 5, and 8 min deposition times in panels A, B, and C, respectively. The mean width, based on 75 particles per sample, was 10, 11, and 11 nm for A, B, and C, respectively. Due to the tip effect, these are larger than the actual particle diameters as confirmed by STM imaging (see text). In Panel D, a graph of the center-to-center distance between nanoparticles vs deposition time is shown. The distances were derived from the SEM images of Ag nanoparticles deposited onto HOPG (×) and ITO (○) and STM data (Δ) of Ag nanoparticles on HOPG. The solid line is a fit to the data (SEM of Ag nanoparticles on HOPG) assuming that the interparticle distance correlates with the inverse square root of deposition time, exclusively.[9]

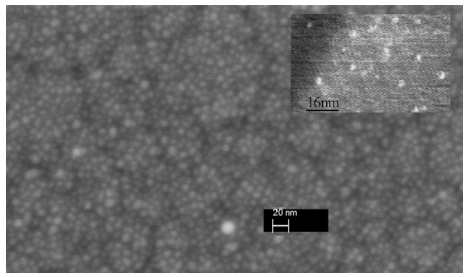


**Figure 4.** SEM image of a relatively high density, nonmetallic film of Ag nanoparticles deposited on ITO on glass. The deposition time for this sample was 7.5 min. In the inset, an STM image of Ag nanoparticles on HOPG is shown. The deposition time was 1 min.

plasmon resonance absorption characteristic of isolated quantum dots is again observable, superimposed over the metal-film type spectrum (red spectrum). The reappearance of the surface plasmon resonance is surprising, as it signifies the start of a second layer of quantum dots, situated atop the close-packed monolayer of quantum dots already on the substrate that is apparently not significantly disturbed by the presence of the second layer and retains its metallic-like optical properties. Clearly, contact between quantum dots does not result in coalescence of the particles; otherwise, the SPR of individual quantum dots would not reappear. Instead, the reappearance of the SPR indicates that the individual quantum dots retain their structures and that the deposited film consists of close-packed, discrete quantum dots.

The presence of discrete particles in the conducting films is confirmed by AFM images shown in Figure 3 where nanoparticles have been deposited on HOPG. Consistent with the optical data, the two-dimensional nature of the films can be seen in these images, and with increasing deposition time, there is an obvious decrease in average interparticle spacing. It is also clear that nanoparticle coalescence is minimal. This is perhaps most evident in the 5 min sample. At 8 min, the nanoparticle spacing is smaller than the resolution of the AFM, so the outlines of individual quantum dots are harder to see, but AFM profiling shows distinct particles. The discrete nature of the conducting nanoparticle films is best demonstrated by the SEM image shown in Figure 4 due to its higher resolution.

In Figure 3, a plot of the interparticle separation, derived from SEM images and STM images of nanoparticles on HOPG and SEM images of nanoparticles on ITO, is shown as a function of deposition time. The solid line is a fit to the data assuming the interparticle distance correlates with the inverse square root of deposition time, exclusively. This is expected when the deposition is purely statistical, which is consistent with these data.[9] At this time, the exact mechanism is not clear, but the lack of coalescence observed is indicative of interparticle repulsion. As the nanoparticles generated by the sputtering source are mostly anions, Coulomb repulsion between particles is very likely to impede particle coalescence and facilitate formation of the two-dimensional, monodispersed nanoparticle ensembles observed. The self-assembly of charged nanoparticles into two-dimensional, monodispersed films has been reported in the formation of Coulomb crystals consisting of well-spaced nanoparticles. [17]

In combination, the SPR, STM, SEM, and AFM results elucidate the mechanism of quantum dot film growth associated with the gas-phase approach. In summary, (1) the approach generates a monodispersed film of quantum dots; (2) the spacing between particles is controllable and steadily decreases with deposition time until, eventually, a monolayer of quantum dots results; (3) after this, if deposition continues, a second layer of quantum dots can be deposited on top of the first; (4) there is no significant amount of particle coalescence and the particles retain their individuality throughout. A remarkable feature of these assemblies is that, at relatively high particle densities, a constant minimum interparticle separation is reached that is relatively large. From STM measurement of many samples, this distance is $10 \pm 2$ nm. As the nanoparticles have diameters of $3.0 \pm 0.5$ (Figure 4 inset), the $10 \pm 2$ nm minimum center-to-center distance corresponds to nontouching, well-separated, nanoparticles. Our results therefore demonstrate the fabrication of two-dimensional solids consisting of close-packed nontouching naked metal quantum dots, the ability to vary the average interparticle separation in such two-dimensional solids, and the possibility of expanding such solids into 3D structures.

The evolution of the conduction characteristics of a Ag quantum dot film during deposition is shown in Figure 5. The current has been plotted as a function of the inverse of the square root of the deposition time, $t^{-1/2}$, which correlates with the average distance between particles (Figure 3 D).[8,9] Thus, the plot illustrates the effect of decreasing the average distance between adjacent quantum dots on the current flow through the quantum dot assembly. Current flow is measured between two Ag electrodes painted onto the substrate surface prior to deposition of the quantum dots. As seen in Figure 5, shortly after deposition is started the onset of current flow occurs. Initially, it increases relatively rapidly ($t^{-1/2} = 0.065$ s$^{-1/2}$) but then increases linearly (on the log scale shown) until $t^{-1/2} \simeq 0.025$ s$^{-1/2}$. In this regime, the interparticle spacing is relatively large initially (Figure 3D), and interparticle tunneling is the only mechanism by which current is expected to flow. The linear trend in the log(current) versus interparticle separation

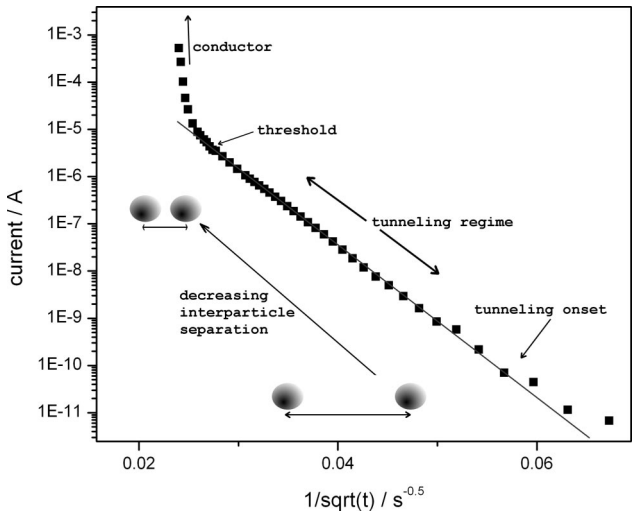


**Figure 5.** Current flow through a two-dimensional ensemble of 3.0 ± 0.5 nm diameter Ag quantum dots is shown as a function of the inverse of the square root of deposition time, $t^{-1/2}$, which is directly proportional to the average interparticle separation.[9] Different conduction mechanisms are labeled adjacent to the interparticle separations where each is prominent. The applied voltage was 1 V.

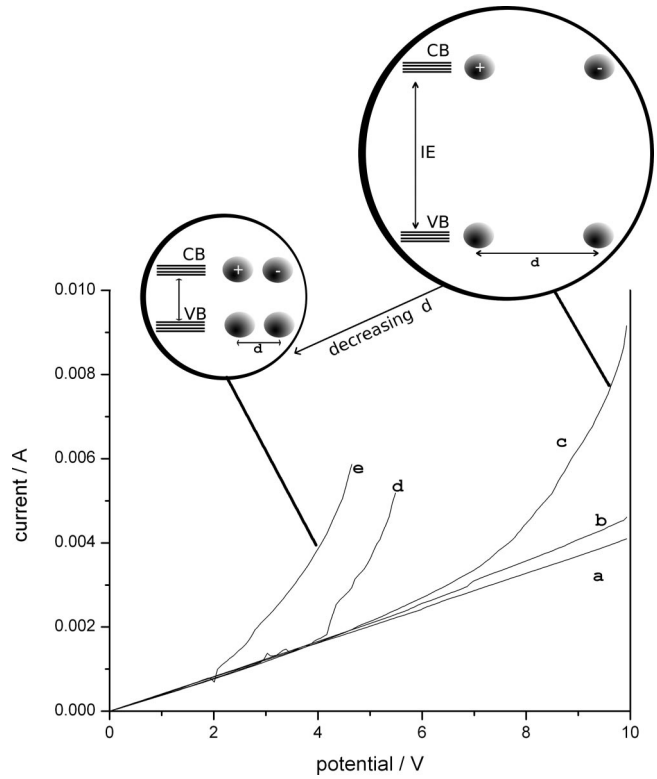


**Figure 6.** Current is shown as a function of the voltage applied across two-dimensional ensembles of 3.0 ± 0.5 nm diameter Ag quantum dots obtained in situ in a vacuum ($10^{-6}$ Torr). The traces a−e correspond to samples with deposition times of 13, 14, 14.5, 15.5, and 17.0 min, respectively. From Figure 3D, the center-to-center spacings are 10.0, 9.7, 9.5, 9.5, and 9.4 nm for traces a−e, respectively, with accuracy of ±2 nm, precision of ±0.2 nm. Each curve has been scaled so that all data can be viewed in one plot. Scaling factors are 60, 25, 6, 5, and 1 for a, b, c, d, and e, respectively. Pictures at the top illustrate the energy gap between conduction and valence bands (CB, VB) for quantum dots with different spacings between them. See text for details.

(i.e., $t^{-1/2}$) plot is characteristic of tunneling current flow.[19,20] The coupling interactions as a prerequisite for tunneling are evident in the interparticle dipolar coupling, the presence of which is responsible for the steady shifting of the SPR to longer wavelengths during this stage of particle deposition, as seen in Figure 2. As interdot separation decreases further, the linearity associated with tunneling current through the quantum dot assembly disappears and a large jump in current flow occurs. Clearly, there is a dramatic change, and another mechanism of charge transport, more efficient than the tunneling of charge between neighboring dots, has become available to the quantum dot ensemble. Candidate mechanisms include percolation, hopping, and/or the onset of an insulator−metal transition.

For nanoparticle-based materials, the finite charging energy of the constituent dots is well-known to manifest enhanced current flow above threshold voltages where charging of the dots becomes possible.[21,22] Above the threshold, it becomes energetically possible to charge each quantum dot in the ensemble, and charge transport via sequential hopping of charge along the full length of the nanoparticle chains between electrodes can occur. This mechanism requires that the voltage drop across each dot exceed the charging energy of the particle. It is unlikely, however, that such charging is responsible for the rapid increase in current observed above the threshold in Figure 5. As mentioned above, the minimum center-to-center distance between particles in the conducting films is 10 ± 2 nm. Given that the electrodes are 3 mm apart, the voltage applied is therefore dropped across 30 000 particles between electrodes. Application of 1 V bias, as in Figure 5, amounts to a 0.03 mV drop per particle, which is insufficient to charge the particles which have a charging energy of 480 ± 50 meV ($E = e^2/4\pi\varepsilon_0\varepsilon d$, where $E$ is the charging energy, $\varepsilon_0$ is vacuum permittivity, $\varepsilon$ is the relative dielectric constant, and $d$ is the particle diameter).[23,24] If the spacing between particles was inhomogeneous, we could consider conduction through a string of larger islands because then the voltage drop per island increases. For 250 islands, for example, the voltage drop is 40 mV per island, which could be observable at room temperature, bearing in mind the effects of thermal broadening. However, the diameter of each island in this case is 1200 nm, and pieces of metal this big have charging energies much too small (1 meV) to present a significant Coulomb blockade that is observable at room temperature. Neither sequential hopping of charge along a chain of dots or along a string of islands is consistent with observation. Accordingly, attributing the rapid increase in current flow (Figure 5) to a Coulomb blockade effect does not seem feasible for the Ag quantum dot ensembles.

The onset of a different conduction mechanism at the threshold in Figure 5 is reflected in the current vs voltage scans shown in Figure 6 for a number of different interparticle separations. When the interparticle separation is large, the plots (Figure 6a and b) are linear. Such Ohmic behavior is expected when tunneling is the dominant mechanism of charge transport, consistent with the linearity of the "tunneling" region labeled in Figure 5. However, when interparticle separation approaches the threshold (Figure 5) non-Ohmic behavior uncharacteristic of tunneling is observed. As seen in Figure 6c,d,e, at low voltage the conductance is still Ohmic, but there is clear deviation at higher voltages where the current increases dramatically. The sigmoidal shapes of these current vs voltage curves contrast the linear behavior observed at larger interparticle spacings where current flow occurs via tunneling, specifically. Clearly, the rapid increase in current at higher voltages corresponds to the presence of an additional conduction mechanism that is more efficient than interparticle tunneling. Percolation, where charges migrate along contiguous metal paths connecting the two

electrodes, gives Ohmic behavior inconsistent with the sigmoidal shape.[25] Hopping, and the associated Coulomb blockade, can produce a threshold but seems to be inconsistent with the voltage drop per particle that is possible in the ensembles, as discussed above. The low fields applied across the films ($\leq 3\ \mu V\ nm^{-1}$) speak against field-assisted processes such as thermionic emission if the voltage drops homogeneously across the film. The results suggest another mechanism.

The naked Ag quantum dot ensembles display unusually strong coupling effects indicative of strong wave function overlap that may explain the conduction characteristics. As seen in the optical spectra in Figure 2, the loss of the plasmon band and the appearance of a metal-like absorbance spectrum occurs at high particle densities where interparticle coupling is strong. This type of transition is atypical of ligated nanoparticle films in their natural state. The ligated films must first be compressed to interparticle separations below ~5 Å for this type of transition to be seen (e.g., compare the noncompressed films of Trudeau vs the compressed films of Collier).[25,26] As the minimum separation in the naked Ag nanoparticle films is $10 \pm 2$ nm (Figure 3D), it suggests that the coupling in these ensembles of naked nanoparticles occurs at much longer distances than observed in the ligated analogues. In light of this strong coupling, we propose that the threshold voltages observed in Figures 5 and 6 correspond to insulator−metal transitions in the quantum dot ensembles.

The change in the conductance behavior of an ensemble of particles as a function of the interparticle separation is described by the Mott model of insulator-to-metal transitions.[1,2] Within the context of the Mott model, at threshold in Figure 5 the interparticle separation is small enough that the overlap of the wave functions on adjacent quantum dots becomes significant and the exchange energy gained from delocalization of the electrons over the film surpasses the charging energy of the particles. The mechanism of charge transport evolves from interparticle tunneling to resonant charge transport, accordingly. Such behavior has been observed previously in two-dimensional ensembles of ligated quantum dots and attributed to charge transport through a network of delocalized orbitals derived from coupling between wave functions of the constituent quantum dots.[27] As interparticle spacing is decreased further, this delocalized network evolves into the conduction band characteristic of the close-packed two-dimensional quantum dot solid. In contrast to many systems, for the naked quantum dot ensembles the insulator-to-metal transition occurs smoothly over a range of interdot spacings, and several measurements were made of the dc current flow through ensembles within the transition region, as seen in Figure 6. In this regime, the ensembles are neither insulators nor conductors but have tunable bandgaps consistent with the Mott model of charge transport.

To elucidate the conduction mechanism further, the temperature dependence of the conduction was measured at two temperatures. In Figure 7, the conductance of quantum dot films at room temperature are compared with analogous data acquired by immersing the films in boiling nitrogen (77 K). As seen, the film with larger interparticle separation (Figure 7b) displays essentially the same Ohmic conductance at both 77 and 300 K. Contraction of the substrate at 77 K is thought to decrease interparticle spacing and manifest a slight increase in current flow as seen. The data are similar to those observed in ligated nanoparticle systems suggesting that the lack of temperature effect can be associated with weak interparticle coupling.[25] Tunneling current is well-known to show little dependence on temperature,[19,20,28] and the result is consistent with interparticle

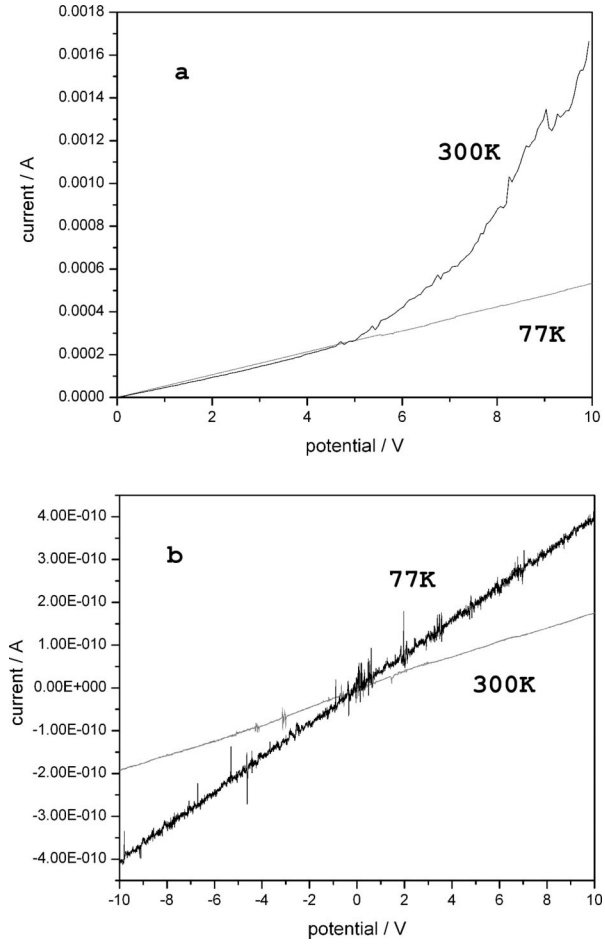


**Figure 7.** Current as a function of the voltage applied across two-dimensional films of Ag quantum dots with diameters of $3.0 \pm 0.5$ nm. The current flow was measured at different temperatures as labeled. The film in Panel b has relatively large interparticle separation so that tunneling is the dominant conduction mechanism. Panel a corresponds to a film with higher particle density, and therefore, a smaller average interparticle separation where resonant current flow is also possible. See text for details.

tunneling being the mechanism by which current flows in these films where interparticle separations are relatively large and coupling is relatively weak, as described above. The second film had interparticle spacing within the proposed insulator−metal transition region. For this film, the room temperature data in Figure 7a display sigmoidal behavior with Ohmic behavior at lower voltage and a threshold for current increase near 5 V. At 77 K, however, the threshold is lost, and purely Ohmic behavior is observed. The change is reversible, and with warming to room temperature, the non-Ohmic conductance is recovered. The result demonstrates clearly that there are two distinct mechanisms of charge transport in these kinds of ensembles. The lack of temperature dependence of the Ohmic part, present at both temperatures, indicates that this is the tunneling contribution to the conductance. The fact that tunneling contributes significantly to the conductance of this ensemble, which is in the insulator−metal transition region, is remarkable and consistent with the naked nanoparticles not coalescing and maintaining significant spacing ($\geq 10 \pm 2$ nm) even in "close-packed" ensembles. The above threshold component is very temperature-dependent and thought to be associated with resonant charge transport through the conduction band. The dramatic loss of the above threshold conductivity at 77 K is thought to result from an Anderson localization process[6]

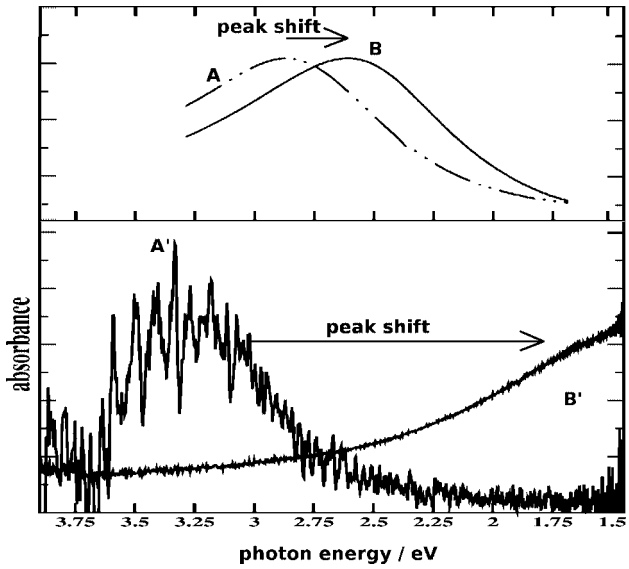


**Figure 8.** Comparison of the absorbance spectra of ligated Ag nanoparticles from the Heath group (top) with the absorbance spectra of the naked nanoparticles from the present work. The peak shift caused by decreased interparticle separation in the thin films is $2.80 - 2.55 = 0.25$ eV for ligated particles and over $3.30 - 1.50 = 1.80$ eV for the naked nanoparticles. The larger peak shift reflects much stronger interparticle coupling in the naked nanoparticle system. See text for details.

in which charge carriers are lost to trap sites within the quantum dot ensemble. In this context, although applying an above bandgap bias ensures charge injection into the conducting orbital network, the probability of successful charge transport across the quantum dot film is determined by the probability of the charge becoming trapped in defect sites. As the detrapping process requisite for current flow is an activated process, charge transport in samples with defects is known to yield a conductance with a significant temperature dependence. Due to packing disorder and a finite distribution in quantum dot size, our nanoparticle ensembles are expected to contain local potential energy minima that function as charge trapping sites, and a temperature dependence like that observed in Figure 7 is expected. Alternatively, it is possible that the threshold has been moved from ~5 V to a much higher value beyond the scannable limit. This would suggest hopping as the charge transport mechanism and raise the question of how voltage is dropped across these nanoparticle ensembles. At this time, evidence speaks against the hopping alternative, but additional work is required to rule out this mechanism entirely.

This first study of both conductance and optical properties of two-dimensional films of naked Ag nanoparticles reveals some surprising results distinct from properties observed in analogous films of ligated nanoparticles. In Figure 8, for example, absorbance data from the Heath group[29] are compared with analogous data for the naked nanoparticle films we have used. For the ligated nanoparticles (curve A), isolated particles in solution have surface plasmon resonances at 2.80 eV. With compression into an ordered Langmuir−Blodgett film (curve B), the wavelength of peak absorbance shifts to 2.55 eV as a result of increased interparticle coupling at shorter interparticle separations.[13,30,31] For the naked nanoparticles, the shift is from 3.30 eV (curve A′) to less than 1.5 eV (curve B′). Although in both cases the nanoparticles are $3.5 \pm 0.5$ nm in diameter, the shift is more than 7 times larger for the naked nanoparticles. The dramatic difference illustrates the magnitude of the ligand effect and its impact on interparticle coupling. Even a ligand monolayer is sufficient to damp interparticle coupling effects almost entirely. To exemplify this further, note that the interparticle separation (edge-to-edge) in the compressed ligated film (curve B) is less than 1.5 nm, while in the naked nanoparticle film (curve B′), the edge-to-edge distance is ~10 nm. Despite the much greater separation, the coupling effect is much stronger in the naked film, as reflected in the much larger shift of the SPR absorbance.

The unusually strong interparticle coupling in the naked nanoparticle systems also manifest conductance properties distinct from those observed in analogous ligated nanoparticle systems. It is remarkable, for example, that tunneling current is observed when interparticle separations are greater than 40 nm, as seen in Figure 5. Although interparticle coupling over these distances is well-known to affect surface plasmon resonances and their associated optical properties,[13,30,31] the manifestation of such long-distance coupling as a tunneling current has not, to our knowledge, been seen previously. The dramatic contrast in the extent of tunneling contributions to current flow in the ligated and naked nanoparticle films is thought to reflect the ligand effect, specifically. The recent work of Cahen and Kahn,[32] for example, shows that monolayers of alkyl ligands can impose a substantial (1.5 eV) activation energy barrier to tunneling current flow. The absence of this barrier in the naked nanoparticle system may explain why tunneling current is a much more dominant feature of the conductance data. Perhaps the largest consequence of the predominance of tunneling in the naked nanoparticle ensembles is that the temperature-dependence data are quite different from those typically observed in ligated nanoparticle systems. The noneffect of temperature on the Ohmic component of the conductance, as seen in Figure 7, is a characteristic of tunneling current, specifically. That the tunneling mechanism accounts for the bulk of the current flow is a novel characteristic of the naked nanoparticle films.

## 4. Summary and Conclusions

In summary, the formation of two-dimensional naked Ag quantum dot ensembles with variable average interparticle spacing and the possibility of extending into 3D architectures are strongly supported by our experimental results. There is no evidence of coalescence, and the interparticle separation appears to have a minimum of $10 \pm 2$ nm, regardless of deposition time and particle density. The optical properties of the nanoparticle ensembles evolve from those characteristic of a collection of coupled surface plasmons to a metallic-like spectrum as the interparticle separation is decreased. This transition to a metal-like state is also seen in the conductance data. The conductance characteristics of these quantum dot ensembles are tunable over the full spectrum from insulator to band gap material to conductor by varying the interparticle separation. The band gap of the material can be varied from 0 to 5 V. There are two distinct conduction mechanisms. When the interparticle separation is large, tunneling is the dominant mechanism of charge transport. Tunneling is observable in all ensembles, even in those that are highly conducting. The second mechanism is more efficient than tunneling and appears when the interparticle separation is relatively small. The evidence we have suggests that strong interparticle coupling effects manifest the emergence of a delocalized conduction band out of the collection of wave functions initially localized on each of the individual naked Ag quantum dots. Both conductance and optical data indicate that the magnitude of interparticle coupling in the naked nanoparticle ensembles is at least 7 times larger than that observed in ligated

nanoparticle systems and occurs over much larger distances. Such strong coupling results in a conductance dominated by tunneling charge transport mechanisms and metallic behavior at interparticle separations of $10 \pm 2$ nm. Both of these are novel features of the naked nanoparticle ensembles that are distinctly different from properties typically observed in ligated systems. These measurements of both optical and conductance data of *naked* nanoparticle ensembles provide new insight into the nature of interparticle coupling and the magnitude of the ligand effect and its impact on optical and conductance properties of nanoparticle ensembles.

**Acknowledgment.** We thank Shelley Ewing for help with the graphics. We thank Armando Marenco and Bernie Kraatz for help with the AFM and SEM images.

## References and Notes

(1) Mott, N. F. *Proc. Phys. Soc. (London)* **1949**, *A62*, 416.
(2) Mott, N. F. *Rev. Mod. Phys.* **1968**, *40* (4), 677–683.
(3) Kim, S. H.; Medeiros-Ribeiro, G.; Ohlberg, D. A. A.; Williams, R. S.; Heath, J. R. *J. Phys. Chem. B* **1999**, *103*, 10341–10347.
(4) Sampaio, J. F.; Beverly, K. C.; Heath, J. R *J. Phys. Chem. B.* **2001**, *105*, 8797–8800.
(5) Beverly, K.; Sampaio, J.; Heath, J. *J. Phys. Chem. B* **2002**, *106* (9), 2131–2135.
(6) Anderson, P. W. *Phys. Rev.* **1958**, *109*, 1429.
(7) Pedersen, D. B.; Wang, S. *J. Phys. Chem. C* **2007**, *111*, 1261–1267.
(8) Pedersen, D. B.; Wang, S.; Paige, M. F.; Leontowich, A. F. G. *J. Phys. Chem. C* **2007**, *111* (15), 5592–5598.
(9) Pedersen, D. B.; Wang, S. *J. Phys. Chem. C* **2007**, *111* (47), 17493–17499.
(10) Liebsch, A. *Phys. Rev. B* **1993**, *48* (15), 11317–11328.
(11) Zhang, X.; Hicks, E. M.; Zhao, J.; Schatz, G. C.; Van Duyne, R. P. *Nano Lett.* **2005**, *5* (7), 1503–1507.
(12) Haynes, C. L.; van Duyne, R. P. *J. Phys. Chem. B* **2001**, *105*, 5599–5611.
(13) Haynes, C. L.; McFarland, A. D.; Zhao, L.; van Duyne, R. P.; Gunnarsson, L.; Prikulis, J.; Kasemo, B.; Kall, M. *J. Phys. Chem. B* **2003**, *107*, 7337–7342.
(14) Su, K. X.; Wei, Q. H.; Zhang, X.; Mock, J. J.; Smith, D. R.; Schultz, S. *Nano Lett.* **2003**, *3* (8), 1087–1090.
(15) Henrichs, S.; Collier, C.; Saykally, R.; Shen, Y.; Heath, J. *J. Am. Chem. Soc.* **2000**, *122* (17), 4077–4083.
(16) Johnson, P. B.; Christy, R. W. *Phys. Rev. B* **1972**, *6* (12), 4370–4379.
(17) P. F. Williams, P. F.; A. Belolipetski, A.; Goussev, A.; M. E. Markes, M. E *Electrochem. Soc. Proc.* **1999**, *99* (22), 189–200.
(18) Tainoff, D.; Bardotti, L.; Tournas, F.; Guiraud, G.; Boisron, O.; Melinon, P. *J. Phys. Chem. C* **2008**, *112* (17), 6842–6849.
(19) Marcus, R. A. *Annu. Rev. Phys. Chem.* **1964**, *15*, 155–196.
(20) Jortner, J.; Bixon, M.; Langenbacher, T.; Michel-Beyerle, M. E. *Proc. Natl. Acad. Sci. U.S.A.* **1998**, *95*, 12759–12765.
(21) Tran, T. B.; Beloborodov, I. S.; Hu, J.; Lin, X. M.; Rosenbaum, T. F.; Jaeger, H. M. *Phys. Rev. B* **2008**, *78* (7), 075437.
(22) Quinn, A. J.; Biancardo, M.; Floyd, L.; Belloni, M.; Ashton, P. R.; Preece, J. A.; Bignozzi, C. A.; Redmond, G. *J. Mater. Chem.* **2005**, *15*, 4403–4407.
(23) Kouwenhoven, L. P.; Marcus, C. M.; McEuen, P. L.; Tarucha, S.; Westervelt, R. M.; Wingreen, N. S. In *Proceedings of the NATO Advanced Study Institute on Mesoscopic Electron Transport*; Kluwer Series E345; Kluwer: Dordrecht, 1997; pp 105−214.
(24) Simon, U. *Nanoparticles: From Theory to Application*; Wiley-VCH, 2004; chapter 5.2, pp 328−367.
(25) Trudeau, P. E.; Orozco, A.; Kwan, E.; Dhirani, A. A. *J. Chem. Phys.* **2002**, *117* (8), 3978–3981.
(26) Collier, C. P.; Saykally, R. J.; Shiang, J. J.; Henrichs, S. E.; Heath, J. R. *Science* **1997**, *277*, 1978–1981.
(27) Remacle, F.; Beverly, K. C.; Heath, J. R.; Levine, R. D. *J. Phys. Chem. B* **2003**, *107*, 13892–13901.
(28) Jortner, J. *J. Chem. Phys.* **1976**, *64*, 4860.
(29) Heath, J. R.; Knobler, C. M.; Leff, D. V. *J. Phys. Chem. B* **1997**, *101*, 189–197.
(30) Zhao, L.; Kelly, K. L.; Schatz, G. C. *J. Phys. Chem. B* **2003**, *107*, 7343–7350.
(31) Kelly, K. L.; Lazarides, A. A.; Schatz, G. C. *Comput. Sci. Eng.* **2001**, *3* (4), 67–73.
(32) Salomon, A.; Boecking, T.; Chan, C. K.; Amy, F.; Girshevitz, O.; Cahen, D.; Kahn, A *Phys. Rev. Lett.* **2005**, *95*, 2668071−4.

JP808516F